A&A 490, 811–815 (2008)
DOI: 10.1051/0004-6361:200810215

Astronomy & Astrophysics

Dynamics of coronal mass ejections

The mass-scaling of the aerodynamic drag

B. Vršnak[1], D. Vrbanec[1], and J. Čalogović[1]

Hvar Observatory, Faculty of Geodesy, Kačićeva 26, 10000 Zagreb, Croatia
e-mail: bvrsnak@geof.hr

Received 18 May 2008 / Accepted 30 July 2008

ABSTRACT

Context. Coronal and interplanetary propagation of coronal mass ejections (CMEs) is strongly affected by aerodynamic drag.
Aims. The dependence of the drag acceleration on the mass of the CMEs is investigated to establish a quantitative empirical relationship, which might be important in semi-empirical space-weather forecasting.
Methods. We employ a large sample of CMEs observed in the radial distance range of 2–30 solar radii by the Large Angle and Spectrometric Coronagraph on board the SoHO mission to statistically analyze the acceleration-velocity relationship in subsamples of various classes of CME masses.
Results. It is demonstrated that the slope and the v-axis intercept of the anti-correlation of the CME acceleration a and velocity v depend on the mean mass of CMEs included in the sample. The slope k of the correlation is less steep for subsamples of higher masses, revealing that massive CMEs are less affected by the aerodynamic drag. Furthermore, it is found that the v-axis intercept is shifted to higher velocities for subsamples of higher masses. This indicates that, on average, the driving force is greater in more massive CMEs.
Conclusions. The empirically established dependence of the $a(v)$ slope on the CME mass is very close to the dependence $k \propto m^{-1/3}$ which follows from the physical characteristics of the aerodynamic drag.

Key words. Sun: coronal mass ejections (CMEs) – Sun: corona – Sun: solar wind – magnetohydrodynamics (MHD)

1. Introduction

Coronal mass ejections (CMEs) are driven by the Lorentz force, which accelerates unstable coronal magnetic structures to velocities sufficient to launch them into the interplanetary space (cf. Forbes 2000). After take-off, the dynamics of CMEs is strongly affected by the interaction of the erupting structure with the ambient magnetoplasma. The expansion of fast CMEs transfers the momentum and energy to the solar wind, whereas in slow CMEs the situation is opposite, i.e., the solar wind transfers the momentum and energy to the ejection.

The CME dynamics sometimes is also affected by interaction with other CMEs (Wang et al. 2005, and references therein). The effects of the CME-CME interaction can be directly measured when two CMEs are launched from the same active region in close succession, in particular in situations where the second CME is faster than the first one. As a result of the interaction, the first CME is additionally accelerated, whereas the second one is decelerated. Wang et al. (2005) have simulated such an interaction numerically, and were able to reproduce in detail the CME-CME interaction event of 20 January 2001. The analysis of the results has shown that in such situations the reconnection plays an important role in the dynamics of the CME pair.

On the other hand, as a result of the CME-wind coupling, eruptions that are faster than the solar wind generally decelerate, whereas those slower than solar wind accelerate. Such a tendency was documented by Gopalswamy et al. (2000) who showed that the velocity distribution of CMEs observed by coronagraphs, spanning from 100 to 3000 km s^{-1} (Yashiro et al. 2004), changes in the interplanetary space, to became grouped around the solar wind speed ($w \approx 400$ km s^{-1}) when measured in situ at 1 AU. Even more direct evidence of the adjustment to the solar wind speed was provided by Manoharan (2006), who measured the interplanetary kinematics of a number of CMEs utilizing radio-scintillation observations.

Effects of the CME-wind coupling also can be measured in the coronagraphic data. Analyzing kinematics of 12 decelerating fast CMEs, Vršnak (2001) demonstrated that the deceleration is speed- and height-dependent. Faster CMEs tend to show stronger deceleration, whereas deceleration decreases with height, i.e., with decreasing ambient density. The analysis was extended by Vršnak et al. (2004a) who studied the acceleration-velocity dependence using a sample of more than 5000 CMEs observed by the Large Angle and Spectrometric Coronagraph (LASCO, Brueckner et al. 1995) on board the Solar and Heliospheric Observatory (SoHO). The analysis presented therein showed a distinct anti-correlation between the CME acceleration a and velocity v, with the v-axis intercept at $v_0 \approx 400$ km s^{-1}.

Such a behavior indicates that motion of CMEs is strongly affected by the "aerodynamic" drag, caused by emission of large-scale large-amplitude MHD waves, which carry away the momentum and energy (Cargill et al. 1996; Cargill 2004). The association of decelerating fast CMEs with type II radio bursts (signatures of shock waves), documented by Gopalswamy et al. (2005), strongly favors such an interpretation. The existence of large-amplitude coronal waves is revealed also by the displacement/relaxation of distant streamers after the CME take-off, as well as by various coronagraphic features suggestive of CME-driven shocks (Sheeley et al. 2000; Vourlidas et al. 2003).

The use of large CME sample in Vršnak et al. (2004a) allowed the decoupling of various parameters affecting the $a(v)$

relationship. The analysis showed that: i) the drag acceleration decreases with radial distance and depends on the size of the CME; ii) in most CMEs the Lorentz force still acts in the considered distance range (2–30 $r_\odot$), being of the order of 10 m s^{-2}.

In this paper we extend the analysis by Vršnak et al. (2004a) by including a still larger sample of LASCO-CMEs, focusing on the effect of the CME mass. Bearing in mind the nature of the aerodynamic drag, it can be presumed that the $a(v)$ relationship should be statistically different for CMEs of different masses. Parametrizing the drag with respect to its size and mass is important for semi-empirical space-weather forecasting of the arrival of ejections at the Earth (see, e.g., Vršnak & Gopalswamy 2002; Michałek et al. 2004; Vršnak & Žic 2007).

2. The data set

In the following analysis we employ data recorded by LASCO from January 1997 to June 2006. The basic characteristics of 11 108 CMEs observed in this period are compiled in the online LASCO CME Catalog (`http://cdaw.gsfc.nasa.gov/CME_list/`; Yashiro et al. 2004), including mass estimates for 6910 events (for details of the procedure we refer to Vourlidas et al. 2000, 2002, and references therein).

From this data set we eliminated all events where either mass or acceleration estimations are marked as uncertain. The final sample used for the analysis contains 3091 CMEs. For each CME from this sample we retrieved from the Catalog the mean velocity v, the mean acceleration a and the mass m of the CME. These data provide a detailed statistical analysis of the $a(v)$ relationship in the LASCO field-of-view (Vršnak et al. 2004a), covering the heliocentric distance range from 2 to 30 solar radii.

Since the following consideration relies on the analysis of the relationship between the CME velocity and acceleration depending on the CME mass, it is important to check if these two kinematic quantities are themselves mass-dependent. The regression analysis shows that the acceleration and mass are not correlated, and that there is only a very weak correlation of the velocity and mass ($v = 180\, m^{0.028\pm0.005}$; correlation coefficient $C = 0.1$). A change of mass by a factor of 100 (range of mean masses of the subsamples treated in Sect. 3) changes the velocity only by 13%, whereas a change by a factor of two results in a velocity difference of only 2%.

3. Results

In Fig. 1a we present the $a(v)$ relationship for all 3091 CMEs, showing that, on average, fast CMEs decelerate, whereas the slow ones accelerate. The anti-correlation of a and v, with the v-axis intercept around 400 km s^{-1} (approximately the slow solar wind speed), shows that the aerodynamic drag plays a distinct role in the dynamics of CMEs in the considered distance range (for details see Vršnak et al. 2004a). Note the lack of data-points at low speeds and negative accelerations, showing that there are practically no slow CMEs that decelerate. On the other hand, there is a considerable fraction of fast CMEs that accelerate, implying that in these events the driving force is still greater than the drag and gravity.

In Fig. 1b we show the $a(v)$ relation separately for two subsamples, one containing 500 CMEs of the smallest masses, and another consisting of 500 events of the largest masses (mean masses $\overline{m} = 7\times10^{10}$ and 7×10^{12} kg, respectively). The two linear least square fits, $a = -kv + a_0$, show that the slope k of the low-mass subsample is steeper than in the large-mass subsample. Following the interpretation of the $a(v)$ anti-correlation in terms of the aerodynamic drag, this indicates that large-mass CMEs are affected by the drag much less than the low-mass events. Note

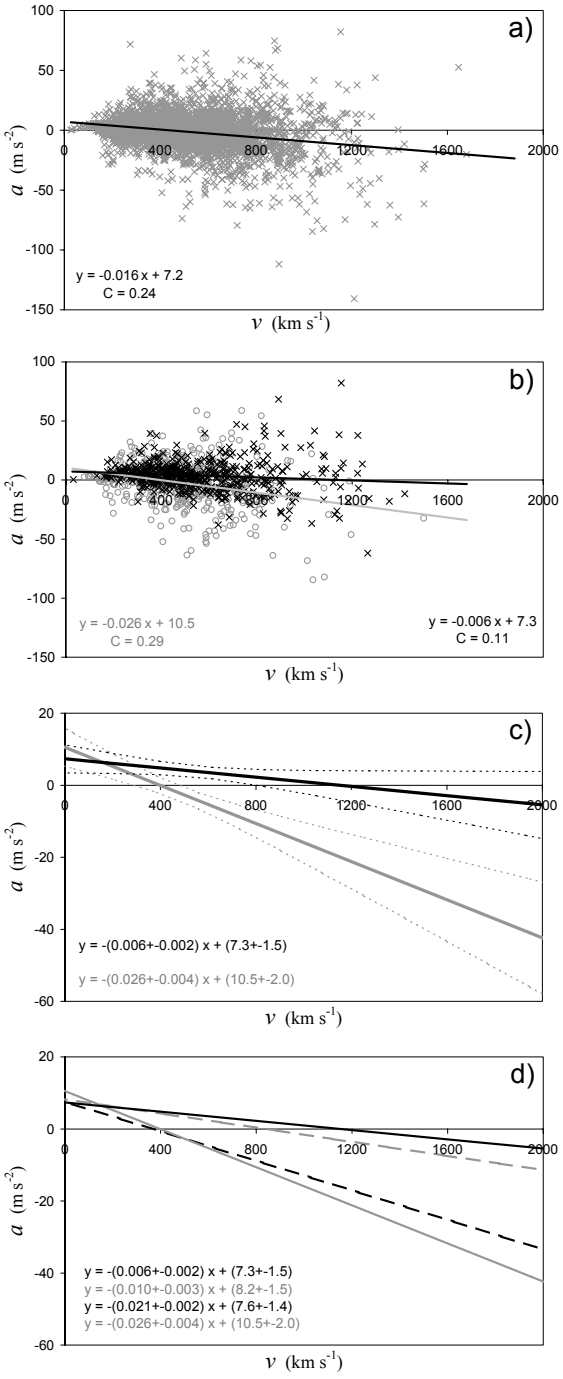

Fig. 1. The CME acceleration versus velocity: **a)** complete data set of 3091 CMEs; **b)** subsample of 500 CMEs of smallest masses (gray circles and gray line) and 500 CMEs of largest masses (black crosses and black line); **c)** the two linear least-square fits from b) shown together with 99% confidence bands (thin dashed); **d)** linear least-square fits for four subsamples of 500 CMEs having average masses of 7×10^{12} kg (full black), 4×10^{12} kg (dashed gray), 7×10^{11} kg (dashed black), and 7×10^{10} kg (full gray). The least-square fit parameters are given in the insets, together with the correlation coefficient C. All correlations have statistical significance $P > 99\%$.

also that the v-axis intercept v_0 is significantly higher for massive CMEs.

The two regression lines from Fig. 1b are shown in Fig. 1c together with the 99% confidence bands, clearly showing that the difference between the two correlations is statistically significant. In Fig. 1d we add two more subsamples with mean masses $\overline{m} = 7\times10^{11}$ kg and 4×10^{12} kg, illustrating a systematic decrease of the slope k with increasing mass.

In order to investigate in more detail the mass-dependence of the slope k and the v-axis intercept v_0, we formed a number of CME subsamples of successively greater mean mass $\overline{m}$. For this purpose we ordered all 3091 CMEs by their mass, and formed subsamples consisting of 500 successive CMEs, where each new subsample was shifted by 100 CMEs toward higher masses. In this way we obtained 27 partly overlapping subsamples (the last one containing only 491 CMEs), characterized by successively greater masses. For each subsample we performed the linear least square fit $a = -kv + a_0$, from which we also derived the v-axis intercept $v_0 = a_0/k$.

The dependence $k(\overline{m})$ is shown Fig. 2a, together with the power-law fit, which reads $k = 10^{-(2.03\pm0.39)} \times \overline{m}^{-(0.23\pm0.03)}$. The results from Fig. 1d are also included (shown by gray squares); in this case the power-law fit adds up to $k = 10^{-(1.31\pm0.89)} \times \overline{m}^{-(0.30\pm0.07)}$. In both representations the decreasing trend of k with increasing mass is evident. In Fig. 2a we also depict the dependencies $k = 0.1\,m^{-1/3}$ and $k = 0.2\,m^{-1/3}$, to ease comparison of the empirical results with the $k(m)$ dependence derived in Sect. 4.

In Fig. 2b we present the dependence $v_0(\overline{m})$. The linear least square fit reads $v_0 = (298 \pm 9) + (1.12 \pm 0.04) \times 10^{-10}\,\overline{m}$. The data clearly show the increase of v_0 with the increasing CME mass. For masses up to $\sim10^{12}$ kg the value of v_0 remains close to the values typical for the slow solar wind speed, $w \sim 300$–400 km s^{-1}, whereas for $\overline{m} > 2\times10^{12}$ kg v_0 becomes significantly larger than these values.

Following Vršnak et al. (2004a), such a deviation could be used to infer the strength of the driving force in the considered height range. The effective driving-force acceleration $a_{\rm L}^* = a_{\rm L} - g$, where $a_{\rm L}$ and g are the Lorentz-force acceleration and the gravity, can be estimated as $a_{\rm L}^* = k\,(v_0 - w)$ (see Sect. 5.3 in Vršnak et al. 2004a). The dependence $a_{\rm L}^*(\overline{m})$ is shown in Fig. 2c, assuming $w = 300$ and 350 km s^{-1}.

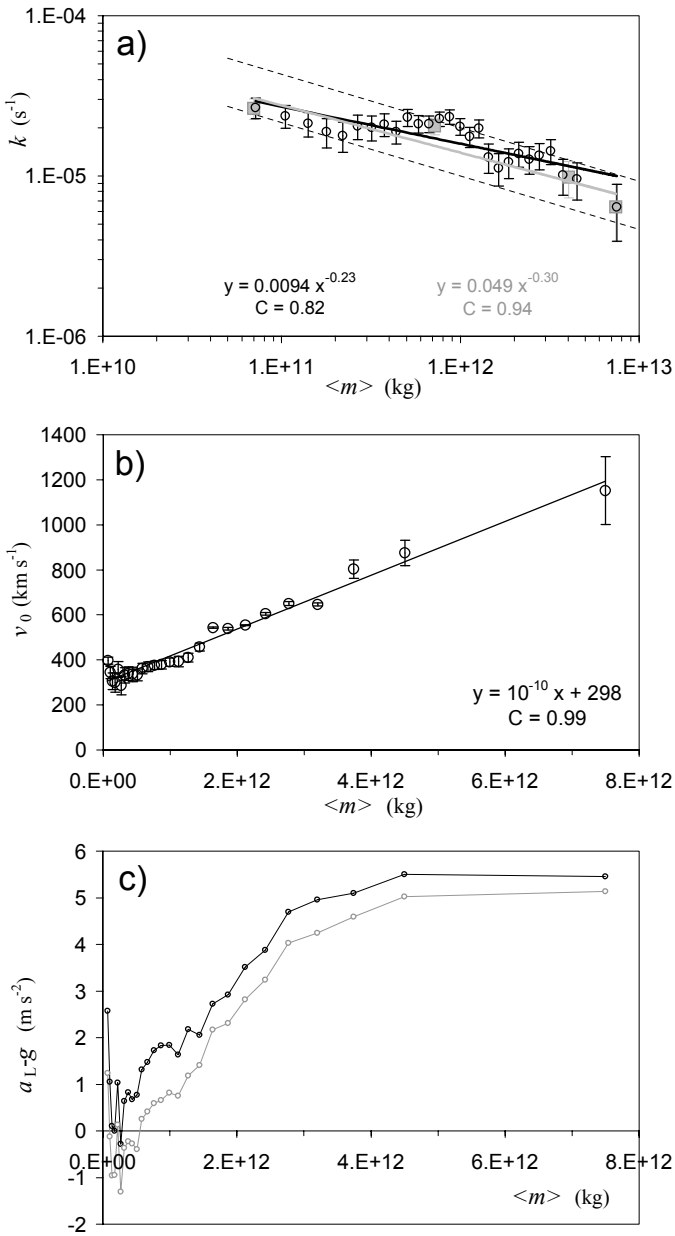

Fig. 2. a) Slope k of the $a(v)$ correlations presented as a function of the mass $\overline{m}$. Circles represent successive subsamples of 500 CMEs. Gray squares represent the four subsamples shown in Fig. 1d. The power-law least square fits are given in the insets. Thin dashed lines represent the dependencies $k = 0.1\,m^{-1/3}$ and $k = 0.2\,m^{-1/3}$. **b)** The v-axis intercept v_0 presented as a function of mass $\overline{m}$. **c)** The effective driving-force acceleration $a_{\rm L} - g$ evaluated using the solar wind speed $w = 300$ and 350 km s^{-1} (black and gray, respectively).

4. Interpretation

The aerodynamic drag is usually expressed in the form (e.g., Cargill et al. 1996; Cargill 2004, and references therein):

$$a = -\gamma(v - w)|v - w|, \tag{1}$$

where v is the CME velocity and w is the ambient solar wind speed. The parameter γ reads:

$$\gamma = c_{\rm d}\frac{A\rho_w}{m}, \tag{2}$$

where $c_{\rm d}$ is the dimensionless drag coefficient (usually having a value of the order of 1; for details see Cargill 2004), A is the effective CME area perpendicular to the direction of propagation, m is the CME mass, and ρ_w represents the ambient solar wind density.

Considering Eqs. (1) and (2), it should be noted that, strictly speaking, they apply only to non-magnetized gas. In the case of magnetized plasma, the coupling between a moving magnetic structure and the ambient magnetoplasma can be quite complex, depending on the mutual orientation of the magnetic field in the two systems. In particular, in the low-viscosity situation, such as we find in the solar corona and interplanetary space, the "magnetic friction" can be quite different from that in the non-magnetized gas (Cargill et al. 1996). For example, under certain circumstances involving magnetic reconnection, the coupling might become very weak ($c_{\rm d} \ll 1$), i.e., the moving structure could propagate practically "frictionless" (for details see Cargill et al. 1996). On the other hand, when the density of the ejection is lower than the ambient density, the drag coefficient can become $c_{\rm d} \gg 1$ (Cargill 2004). Nevertheless, both Cargill et al. (1996) and Cargill (2004) have shown that the

interaction of the moving magnetic structure and the ambient magnetoplasma can be very well reproduced by the functional form given by Eqs. (1) and (2).

Given that any least square fit to the $a(v)$ data set by definition has to pass through the point defined by the average values $(\overline{a}, \overline{v})$, for the fit of the functional form given by Eq. (1) we can write $\overline{a} = -\gamma(\overline{v} - w)|\overline{v} - w|$. Analogously, for the linear approximation of Eq. (1),

$$a = -k(v - w), \tag{3}$$

one finds $\overline{a} = -k(\overline{v} - w)$. Thus, the linear-fit slope k can be expressed as

$$k = \gamma|\overline{v} - w| = \frac{c_{\rm d}A}{m}\rho_w|\overline{v} - w|. \tag{4}$$

Equation (1), as well as Eq. (3), show that in the absence of other forces the intercept with the v-axis should represent the solar wind speed. Furthermore, according to Eq. (2), the slope of the $a(v)$ correlation is inversely proportional to the CME mass and proportional to the CME area. Writing for the CME mass $m = \rho_{\rm CME}V$, where V and $\rho_{\rm CME}$ are the CME volume and average density, we get:

$$\frac{A}{m} = \frac{A}{V\rho_{\rm CME}} \sim V^{-1/3}\rho_{\rm CME}^{-1} \propto m^{-1/3}, \tag{5}$$

where we have taken approximately $A \sim V^{2/3}$. Combining Eqs. (4) and (5), we get that the slope of the $a(v)$ correlation scales as $k \propto m^{-1/3}$. This is quite close to the power-law slopes 0.23 and 0.30 which we obtained in Sect. 3 (see Fig. 2a).

Thus, the expression for the slope k can be written as $k = \alpha\, m^{-1/3}$, where $\alpha = c_{\rm d}\rho_w^{1/3}(\rho_w/\rho_{\rm CME})^{2/3}|\overline{v} - w|$. Considering various coronal density models (see, e.g., Vršnak et al. 2004b, and references therein), we can take that at $R \sim 10$ the coronal number density ranges between $n_w \sim 10^4$ and 10^5 cm^{-3}. Note that changing the density by a factor of 10 changes α only by a factor of 2. Since the mean CME speed in our sample adds up to $\overline{v} = 520$ km s^{-1}, we can take $\overline{v} - w \sim 100$–$200$ km s^{-1}. Assuming $\rho_w/\rho_{\rm CME} \sim 1/10$, we get $\alpha \sim 0.05$–0.2. Bearing in mind the order-of-magnitude nature of the presented estimate, such values are consistent with the observations shown in Fig. 2a, where dependencies $k = 0.1\, m^{-1/3}$ and $k = 0.2\, m^{-1/3}$ are drawn to ease comparison.

5. Discussion

There are various effects which might influence the empirical results presented in Sect. 3. Certainly the most important are projection effects, since they affect the measured kinematical parameters (Burkepile et al. 2004; Schwenn et al. 2005; Vršnak et al. 2007; Howard et al. 2008).

Given that the projected velocity (and thus also the acceleration $|a|$) is lower than the real value (Schwenn et al. 2005; Vršnak et al. 2007), the projection effect manifests in $a(v)$ graphs in two different ways. In the $a > 0$ domain the data-points are shifted in the left-downward direction relative to the true positions, whereas in the $a < 0$ domain they are shifted in the left-upward direction. This implies that the evaluated slopes k and the v-axis intercepts v_0 of the $a(v)$ correlations (and thus the effective driving force acceleration $a_{\rm L} - g$), are underestimated to a certain degree. Yet, given that measured speeds of CMEs launched from the limb are higher on average only by $\lesssim$50% than in CMEs launched from the central parts of the disc (Vršnak et al. 2007),

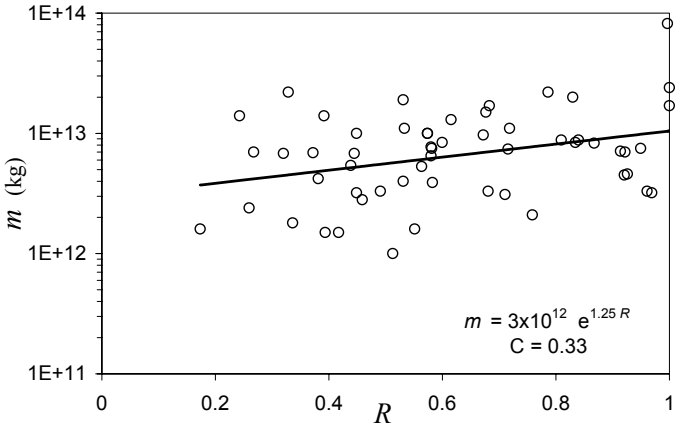

Fig. 3. Dependence of the CME mass estimates on the position of the source region ($R = 1$ represents solar limb).

the values of $a_{\rm L} - g$ derived in Sect. 3 are probably not underestimated by more than a few tens of percents, whereas the underestimation of k is probably even smaller.

Another effect of the position of the CME source region is related to the mass estimate. In Fig. 3 we show the estimated CME masses versus the source region position. This sample, containing 56 events for which the CME source location could be unambiguously determined, is based on the CME data set complied by Schwenn et al. (2005). The exponential fit has a correlation coefficient $C = 0.33$ and the statistical significance is greater than 98%. Figure 3 shows that, on average, masses of CMEs launched from regions close to the disc center might be underestimated by a factor ~2. Such a centre-to-limb tendency is not surprising, given the nature of the Thompson scattering being most effective in the plane-of-sky.

Both aspects of the projection effects influence the results presented in Fig. 2. First, taking into account Fig. 3, the low-mass subsamples probably contain larger numbers of CMEs launched from regions close to the disc center, i.e., in these subsamples the mean mass is probably underestimated, as are the slopes of the $a(v)$ correlations. Thus, these data points should be shifted in Fig. 2a in the right-upward direction, which would increase the power-law slope. This might explain the deviation of low-mass data-points from the power-law in Fig. 2a. Increasing values of k and m by a factor of two in the low-mass subsamples (say, $m < 5\times10^{11}$ kg) would roughly adjust the power-law slope to the expected one, $m^{-1/3}$, depicted by the thin-dashed lines in Fig. 2a.

A good match of the empirical dependence $k(m)$ with the theoretical one implies also that the magnetic friction acting on CMEs can be described by Eqs. (1) and (2). It also means that in the considered distance range the drag coefficient $c_{\rm d}$ is roughly constant, which is consistent with results of the full MHD calculation presented by Cargill (2004). Furthermore, it implies that the majority of CMEs has an average density higher than the ambient corona. Otherwise, tenuous CMEs whose motion should be characterized by $c_{\rm d} \gg 1$ (Cargill 2004) would increase values of the slope k for low-mass subsamples, which would make the $k(m)$ slope steeper than observed.

Finally, one should consider the effect of a non-negligible driving force. It is possible that the effective driving force $a_{\rm L} - g$ is on average stronger in faster CMEs (note a greater scatter of accelerations at higher velocities in Fig. 1a). This would lead to a decrease of evaluated slopes k of $a(v)$ correlations, i.e., the true values of the drag parameter k might be higher than presented

in Fig. 2a. However, since there is only a very weak statistical dependence between the CME speed and mass, this effect would be approximately the same for all CME masses, i.e., the slope of the power-law fit $k(m)$ would not be affected significantly. On the other hand, the estimation of the driving force itself might be affected, since true values of the v-axis intercept v_0 would be lower, implying that the driving force is somewhat weaker than estimated.

In this respect, it should be also noted that in estimating $a_L - g$ we used for the solar wind speed $w = 300$ and 350 km s^{-1}. Here we were guided by the fact that CMEs are mostly launched from active regions, implying that the majority of CMEs propagates through the slow solar wind. However, in the considered height range, the slow solar wind speed might be lower than we assumed in our estimation of $a_L - g$ (see Figs. 6a and b in Sheeley et al. 1997). That would mean that the estimated values for $a_L - g$ might be underestimated, say, by a factor of two. On the other hand, if we would apply higher solar wind speeds (bearing in mind that a fraction of CMEs propagates through the fast solar wind streams), the true values of $a_L - g$ would be lower. In CMEs of lowest masses, that would result in negative $a_L - g$ (see Fig. 2c), implying that low-mass CMEs are decelerated not only by the magnetic friction, but also by $a_L - g < 0$. Such a situation can be foreseen theoretically (see the green curve in Fig. 5b of Vršnak 2008), and seems to be confirmed observationally (see, e.g., Wang & Sheeley 2002).

6. Conclusion

Measurements in the radial distance range 3–30 $r_\odot$ show that after the acceleration stage the CME dynamics becomes strongly affected by the aerodynamic drag. Vršnak et al. (2004a) have shown that the drag acceleration decreases with height and depends on the size of the CME. This implicitly includes that the drag is mass/size dependent (see Sect. 5.2 in Vršnak et al. 2004a). In this paper we have extended the analysis, to establish an explicit empirical relationship between the drag acceleration and the CME mass.

The empirical results show that the dependence of the drag acceleration on the CME mass follows quite closely the theoretically expected scaling $m^{-1/3}$. A somewhat less steep trend than expected can be explained by the projection effects affecting the CME kinematics and the mass estimate.

Finally, our analysis reveals that in the distance range 2–30 solar radii the Lorentz force is of the order of 1–10 m s^{-2}. The data indicate that the Lorentz force is stronger in CMEs of higher masses.

Acknowledgements. We are grateful to the LASCO-SoHO and GOES teams for operating the instruments and performing the basic data reduction. We are especially grateful to Nat Gopalswamy, Seiji Yashiro, Grzegorz Michałek and their colleagues for compiling the online LASCO CME Catalog and to the referee (S. T. Wu) whose comments and suggestions led to a significant improvement of the paper.

References

Brueckner, G. E., Howard, R. A., Koomen, M. J., et al. 1995, Sol. Phys., 162, 357
Burkepile, J. T., Hundhausen, A. J., Stanger, A. L., St. Cyr, O. C., & Seiden, J. A. 2004, J. Geophys. Res., 109
Cargill, P. J. 2004, Sol. Phys., 221, 135
Cargill, P. J., Chen, J., Spicer, D. S., & Zalesak, S. T. 1996, J. Geophys. Res., 101, 4855
Forbes, T. G. 2000, J. Geophys. Res., 105, 23153
Gopalswamy, N., Lara, A., Lepping, R. P., et al. 2000, Geophys. Res. Lett., 27, 145
Gopalswamy, N., Aguilar-Rodriguez, E., Yashiro, S., et al. 2005, J. Geophys. Res., 110, A12S07
Howard, T. A., Nandy, D., & Koepke, A. C. 2008, J. Geophys. Res., Space Phys., 113, 1104
Manoharan, P. K. 2006, Sol. Phys., 235, 345
Michałek, G., Gopalswamy, N., Lara, A., & Manoharan, P. K. 2004, A&A, 423, 729
Schwenn, R., dal Lago, A., Huttunen, E., & Gonzalez, W. D. 2005, Ann. Geophys., 23, 1033
Sheeley, N. R., Hakala, W. N., & Wang, Y.-M. 2000, J. Geophys. Res., 105, 5081
Sheeley, Jr., N. R., Wang, Y.-M., Hawley, S. H., et al. 1997, ApJ, 484, 472
Vourlidas, A., Subramanian, P., Dere, K. P., & Howard, R. A. 2000, ApJ, 534, 456
Vourlidas, A., Buzasi, D., Howard, R. A., & Esfandiari, E. 2002, in Solar Variability: From Core to Outer Frontiers, ed. J. Kuijpers, ESA SP, 506, 91
Vourlidas, A., Wu, S. T., Wang, A. H., Subramanian, P., & Howard, R. A. 2003, ApJ, 598, 1392
Vršnak, B. 2001, Sol. Phys., 202, 173
Vršnak, B. 2008, Ann. Geophys., 25, in press
Vršnak, B., & Gopalswamy, N. 2002, J. Geophys. Res., Space Phys., 107, 1019
Vršnak, B., & Žic, T. 2007, A&A, 472, 937
Vršnak, B., Ruždjak, D., Sudar, D., & Gopalswamy, N. 2004a, A&A, 423, 717
Vršnak, B., Magdalenić, J., & Zlobec, P. 2004b, A&A, 413, 753
Vršnak, B., Sudar, D., Ruždjak, D., & Žic, T. 2007, A&A, 469, 339
Wang, A. H., Wu, S. T., & Gopalswamy, N. 2005, Geophys. Monograph Ser., 156, GM21
Wang, Y.-M., & Sheeley, Jr., N. R. 2002, ApJ, 567, 1211
Yashiro, S., Gopalswamy, N., Michalek, G., et al. 2004, J. Geophys. Res., Space Phys., 109, 7105